Systems/Circuits

Control of Spike Transfer at Hippocampal Mossy Fiber Synapses *In Vivo* by $GABA_A$ and $GABA_B$ Receptor-Mediated Inhibition

Stefano Zucca,* Marilena Griguoli,* Meryl Malézieux, Noëlle Grosjean, Mario Carta, and Christophe Mulle
Interdisciplinary Institute for Neuroscience, CNRS, Unité Mixte de Recherche 5297, University of Bordeaux, F-33000 Bordeaux, France

Despite extensive studies in hippocampal slices and incentive from computational theories, the synaptic mechanisms underlying information transfer at mossy fiber (mf) connections between the dentate gyrus (DG) and CA3 neurons *in vivo* are still elusive. Here we used an optogenetic approach in mice to selectively target and control the activity of DG granule cells (GCs) while performing whole-cell and juxtacellular recordings of CA3 neurons *in vivo*. In CA3 pyramidal cells (PCs), mf–CA3 synaptic responses consisted predominantly of an IPSP at low stimulation frequency (0.05 Hz). Upon increasing the frequency of stimulation, a biphasic response was observed consisting of a brief mf EPSP followed by an inhibitory response lasting on the order of 100 ms. Spike transfer at DG–CA3 interneurons recorded in the juxtacellular mode was efficient at low presynaptic stimulation frequency and appeared insensitive to an increased frequency of GC activity. Overall, this resulted in a robust and slow feedforward inhibition of spike transfer at mf–CA3 pyramidal cell synapses. Short-term plasticity of EPSPs with increasing frequency of presynaptic activity allowed inhibition to be overcome to reach spike discharge in CA3 PCs. Whereas the activation of $GABA_A$ receptors was responsible for the direct inhibition of light-evoked spike responses, the slow inhibition of spiking activity required the activation of $GABA_B$ receptors in CA3 PCs. The slow inhibitory response defined an optimum frequency of presynaptic activity for spike transfer at ~10 Hz. Altogether these properties define the temporal rules for efficient information transfer at DG–CA3 synaptic connections in the intact circuit.

Key words: CA3; dentate gyrus; feedforward inhibition; hippocampus; *in vivo*; synapse

Significance Statement

Activity-dependent changes in synaptic strength constitute a basic mechanism for memory. Synapses from the dentate gyrus (DG) to the CA3 area of the hippocampus are distinctive for their prominent short-term plasticity, as studied in slices. Plasticity of DG–CA3 connections may assist in the encoding of precise memory in the CA3 network. Here we characterize DG–CA3 synaptic transmission *in vivo* using targeted optogenetic activation of DG granule cells while recording in whole-cell patch-clamp and juxtacellular configuration from CA3 pyramidal cells and interneurons. We show that, *in vivo*, short-term plasticity of excitatory inputs to CA3 pyramidal cells combines with robust feedforward inhibition mediated by both $GABA_A$ and $GABA_B$ receptors to control the efficacy and temporal rules for information transfer at DG–CA3 connections.

Introduction

On theoretical grounds, the architecture of hippocampal CA3 circuits appears well adapted for the rapid storage and retrieval of associative memories (for review, see Kesner and Rolls, 2015). The two major features of CA3 circuits consist of the extensive excitatory interconnections between CA3 pyramidal cells (PCs) through associational/commissural fibers, which create the anatomical basis for the autoassociative network, and the sparse but

Received June 28, 2016; revised Nov. 2, 2016; accepted Nov. 20, 2016.

Author contributions: S.Z., M.G., and C.M. designed research; S.Z., M.G., M.M., and M.C. performed research; S.Z., M.G., M.M., N.G., M.C., and C.M. analyzed data; S.Z., M.G., and C.M. wrote the paper.

This study was supported by the Centre National de la Recherche Scientifique (CNRS), the European Commission (SyMBaD Marie Curie ITN FP7/2007–2013 Grant agreement no. 238608, fellowship to S.Z.), the Agence Nationale de la Recherche (contract HIPPENCODE), and the LabEx BRAIN. We thank Jerôme Epsztein for fruitful initial discussions and help with *in vivo* patch-clamp recordings; François Georges and Delphine Girard for their help with *in vivo* pharmacological experiments; and Adam Gorlewicz for image acquisition of reconstructed neurons. We also thank Virginie Labrousse for help with confocal microscopy, which was performed at the Bordeaux Imaging Center, a service unit of the CNRS-INSERM and Bordeaux University, and member of the national infrastructure France BioImaging. In addition, we thank Elisabeth Normand, Audrey Lacquemant, and Amandine Gautier for taking care of the mice.

*S.Z. and M.G. are equal first authors.

The authors declare no competing financial interests.

Correspondence should be addressed to Christophe Mulle, University of Bordeaux, Interdisciplinary Institute for Neuroscience, CNRS UMR 5297, F-33000 Bordeaux, France. E-mail: christophe.mulle@u-bordeaux.fr.

DOI:10.1523/JNEUROSCI.2057-16.2016

 0270-6474/17/370587-12$15.00/0

powerful connections from the dentate gyrus (DG) through mossy fiber (mf) synapses, which are proposed to assist in pattern completion and pattern separation (Guzowski et al., 2004; Rolls and Treves, 2011). DG granule cells (GCs) send unmyelinated mf axons to the stratum lucidum, where giant mossy fiber boutons make synaptic contacts with thorny excrescences on basal dendrites of CA3 PCs (Chicurel and Harris, 1992; Rollenhagen et al., 2007; Wilke et al., 2013). Filopodial extensions of mf terminals and en passant synapses provide monosynaptic innervation to local interneurons (INs; Szabadics and Soltesz, 2009), creating a robust feedforward inhibitory circuit (Mori et al., 2004; Torborg et al., 2010). Spike transfer at DG–CA3 connections depends on a balance between direct excitation and feedforward inhibition, both of which are under the control of different short-term plasticity mechanisms (Nicoll and Schmitz, 2005; Evstratova and Tóth, 2014). In slice recordings, with a low frequency of presynaptic GC activity (<0.1 Hz), excitatory synaptic potentials (mf-CA3 EPSPs) have small amplitudes, because of a very low release probability at individual release sites ($p < 0.01$; Lanore et al., 2012), and are insufficient to discharge CA3 PCs. When GCs increase tonic low-frequency firing rate from 0.05 Hz up to theta range frequency or during trains of spikes (with frequencies from 10 to 100 Hz; Nicoll and Schmitz, 2005), synaptic responses in single mf–CA3 PC synapses are capable of triggering postsynaptic action potentials (Sachidhanandam et al., 2009). Hence, the pattern of presynaptic activity can induce prominent short-term plasticity making mf–CA3 synapses work as a "conditional detonator" synapse (Henze et al., 2002). Although synaptic transmission and plasticity at DG–CA3 synapses have been widely studied *in vitro* (Nicoll and Schmitz, 2005; Evstratova and Tóth, 2014; Cherubini and Miles, 2015), how these events operate in vivo are less clear (Henze et al., 2002; Klausnitzer and Manahan-Vaughan, 2008), thus limiting our understanding of the mf synaptic contribution to CA3 network function. It is therefore important to study the functional properties of mf–CA3 synapses *in vivo*. In the present article, we aimed at directly characterizing synaptic transmission rules at mf–CA3 neurons *in vivo* and at understanding how different presynaptic firing modalities (tonic low frequency vs trains of action potentials) control information transfer in the CA3 circuit. To this end, we used an optogenetic approach to selectively target and control the activity of a few GCs while performing single-cell recordings from CA3 neurons in anesthetized mice. We found that mf–CA3 PC synapses exhibited prominent short-term plasticity, as was the case *in vitro*. We show that the local feedforward inhibitory circuits tightly control information transfer at mf–CA3 synapses and that this requires the activation of both $GABA_A$ and $GABA_B$ receptors in CA3 PCs. The 100-ms-long inhibition mediated by $GABA_B$ receptors appears to play an important part in defining the temporal rules for efficient spike transfer at DG–CA3 connections in the intact brain.

Materials and Methods

Mice and in vivo *viral infection.* Male POMC-Cre mice (https://www.jax.org/strain/005965) were used in the present study. All experimental procedures related to the use of mice were conducted according to the guidelines of the University of Bordeaux/CNRS Animal Care and Use Committee. Adeno-associated virus (AAV) serotype 2/9 containing channelrhodopsin-2 [ChR2; AAV-DIO-ChR2(H134R)-enhanced yellow fluorescent protein (EYFP)] was obtained from the University of Pennsylvania Gene Therapy Program (Philadelphia, PA), with genomic titers of 2.6×10^{13} particles/ml. Viral vectors were bilaterally injected in the dorsal DG (−1.8 mm posterior to bregma; ±1.2 mm lateral of bregma; and −1.9 mm ventral from brain surface) of POMC-Cre mice, expressing Cre-recombinase in a subpopulation of DG cells (Gao et al., 2007) between postnatal days 14 and 16. The injection volume and flow rate (~250 nl at 50 nl/min) were controlled with an injection pump (World Precision Instruments). After a minimum of 21 d for protein expression, mice were used for experiments.

Slice electrophysiology. Slice electrophysiology was performed from parasagittal hippocampal slices as described previously (Sachidhanandam et al., 2009). Microelectrodes (3–5 MΩ) were prepared from borosilicate glass capillaries (Harvard Apparatus) using a P-97 puller (Sutter Instrument). For voltage-clamp experiments, pipettes were filled with an intracellular solution containing the following (in mM): 140 Cs methanesulfonate, 4 NaCl, 10 HEPES, 0.2 EGTA, 2 MgCl2, 3 ATP-Na, 5 phosphocreatine, at 0.33 GTP, at 280–300 mOsm, pH 7.2–7.3, adjusted with KOH. For current-clamp experiments, the following internal solution was used (in mM): 120 K-methanesulfonate, 20 KCl, 10 HEPES, 10 EGTA, 2 MgCl2, and 2 Na-ATP, at 290–300 mOsm, pH 7.2–7.3, adjusted with KOH. To monitor the series resistance, a hyperpolarizing voltage step (−10 mV, 50 ms) was applied at the beginning of each recording. Series resistances varied between 10 and 20 MΩ, and when these changed by >20%, recordings were discarded. Measurements of membrane potentials were not corrected for the liquid junction potential error. Data were acquired with an EPC 10 amplifier (HEKA Elektronik), filtered at 2.9 kHz with a Bessel filter, digitized at 10 kHz, and stored on a personal computer for off-line analysis using custom-made macros (IGOR PRO 5.0, WaveMetrics). For optogenetic experiments, $ChR2^+$ DG GCs were activated with 5 ms pulses of blue light generated by a 473 nm LED (pE1, CoolLED) under the control of the digital output of the amplifier. Light-evoked mf–CA3 EPSCs were recorded in voltage-clamp conditions at −70 mV at 34°C. Changes in mf–CA3 synaptic responses were assessed by increasing the stimulation frequency from a basal rate of 0.1 Hz (30 stimuli) to 1 Hz (30 stimuli) and 3 Hz (30 stimuli), and referred as tonic low-frequency facilitation, or during bursts of presynaptic stimulation consisting of four to five trains of 10 light stimulations delivered at 25 and 40 Hz.

In vivo *electrophysiology.* For *in vivo* electrophysiology, surgeries and electrophysiological recordings were performed under isoflurane anesthesia. In a subset of experiments ($n = 3$ mice), a mix of ketamine (100 mg/kg) and xylazine (15 mg/kg) was injected intraperitoneally to induce anesthesia before surgery and during juxtacellular recordings and were compared with those obtained in the presence of isoflurane anesthesia. Two craniotomies for the stimulating and recording sites were drilled between −1.8 and −2.3 mm posterior from bregma, and lateral coordinates were adjusted after extracellular mapping to locate the GC layer or CA3 pyramidal cell layer. Temperature was maintained between 36–37°C using a feedback-controlled heating pad (FHC). Recordings were obtained with a Multiclamp 700B amplifier connected to the Digidata 1440A system. Data were acquired with pClamp 10 (Molecular Devices), digitized at 10 kHz, filtered at 3 kHz, and analyzed off-line with Clampfit 10.4 (Molecular Devices). Activation of $ChR2^+$ GCs was achieved with a 50 mW, 473 nm laser (Shanghai Dream Lasers Technology) delivered through an optic fiber [200 μm, 0.22 numerical aperture (NA)] inserted into the dorsal DG, and positioned with a 20° angle above the dendrites of GCs in the molecular layer. Pulses of blue light (5 ms) were externally triggered using pClamp (Molecular Devices). The following light stimulations protocols were used: 0.05 Hz (baseline, 10 stimuli); 1, 3, and 10 Hz (60 stimuli); and five trains (repeated every 30 s) consisting of 10 light pulses delivered at 20 and 40 Hz.

Extracellular recordings of field potentials were obtained with glass electrodes prepared with a vertical puller PC-10 (Narishige), and the tip was broken to obtain a resistance between 1 and 3 MΩ. Electrodes were filled with a standard Ringer's solution containing the following (in mM): 135 NaCl, 5.4 KCl, 5 HEPES, 1.8 CaCl2, and 1 MgCl2. Changes in field EPSPs (fEPSPs) were measured in terms of slope change and were normalized for the slope values obtained at 0.05 Hz.

Whole-cell patch-clamp recordings were achieved using a standard blind-patch approach as previously described (Margrie et al., 2002; Lee et al., 2009). Electrodes used for whole-cell recordings were prepared before the beginning of electrophysiology experiments, had a resistance between 4 and 7 MΩ, and were filled with a solution containing 120 mM K-methanesulfonate, 20 KCl, 10 HEPES, 10 EGTA, 2 MgCl2, and 2 Na-

ATP, at 290–300 mOsm and pH 7.2–7.3 adjusted with KOH. The intracellular solution was supplemented with 0.2% (w/v) biocytin for *post hoc* cellular identification and morphological reconstruction. Resting membrane potential (RMP) was noted immediately upon achieving whole-cell configuration. Only GCs that showed initial RMP values less than or equal to −60 mV *in vivo* were included in the study. At the end of each recording, the injection of biocytin was achieved by applying positive current pulses (0.5–1 nA, 500 ms, for 5–10 min) through the bridge circuitry of the amplifier. Access resistance and membrane capacitance of the cells were monitored on-line with the membrane test feature of the acquisition software and analyzed off-line. The mean access resistance was 48.8 ± 3.2 MΩ (range, 10.0–89 MΩ; 26 cells). The spontaneous firing frequency of CA3 neurons was estimated during a 1–2 min interval before any stimulation, and spikes during bursts of action potentials were counted as single events (Pernía-Andrade and Jonas, 2014). Bursting behavior of CA3 PCs was assessed using a detection threshold function with Clampfit; a burst was defined as a series of two or more spikes delimited within an interval of 50 ms, both in juxtacellular and whole-cell patch-clamp recordings. The EPSP and IPSP amplitudes were quantified by measuring the peak of the synaptic response obtained from the average trace of all the sweeps recorded at different frequencies. The duration of IPSP for patch-clamp recordings was measured from the onset of the biphasic synaptic response to baseline return values of pure inhibitory response obtained in response to 0.05–10 Hz stimulation. The duration of the EPSP was measured from the onset of the biphasic synaptic response to the theoretical return values of the excitatory component of the biphasic response obtained after 10 Hz stimulation.

Juxtacellular recordings of neuronal firing were obtained using glass electrodes (4–7 MΩ) filled with either Ringer's solution or intracellular solution (attempts at obtaining successful whole-cell patch-clamp recordings). Spike discharge probability was measured within a 30 ms interval from the beginning of the light pulse during tonic low frequencies of stimulation (0.05–10 Hz) and between light pulses during trains at 20 and 40 Hz. This interval has been chosen by considering the latency (5.1 ± 0.7 ms) plus the duration of the EPSP (19.2 ± 5.7 ms; $n = 8$) measured during patch-clamp recordings. Inhibition in juxtacellular recordings was defined as an epoch of at least 10 bins (5 ms per bin) in which the mean count per bin was at least 35% less than baseline (mean of 100 ms before light pulse). In recordings combined with the local application of drugs, the distance between recording and ejection pipettes ranged between 90 and 190 μm. Local application of drugs *in vivo* was performed by pressure application (10 ms, 20 psi, repeated 8–10 times) through a glass ejection pipette (tip diameter, between 30 and 40 μm) connected to a picospritzer (Parker) and glued to a sharp recording electrode (30–40 MΩ; Georges and Aston-Jones, 2002). Drug concentrations were chosen based on previous studies showing efficient modulation of neuronal firing following local application of GABAergic antagonists *in vivo* (Paladini and Tepper, 1999; Chadderton et al., 2004). Changes in firing rate following optical stimulation of GCs (1 Hz) were recorded before and after drug application (onset of the effect for: CGP-55845, 1077 ± 237 s, $n = 7$; gabazine, 206 ± 36 s, $n = 8$).

Immunohistochemistry and image analysis. Brains were processed for *post hoc* identification of ChR2$^+$ GCs and to recover the fluorescence of neurons filled with biocytin during *in vivo* whole-cell patch-clamp recordings. To estimate the number of ChR2$^+$ GCs, brains were removed from the skull, postfixed for 48 h in 4% paraformaldehyde (PFA), washed in PBS, and sectioned at 40 μm with a vibratome. Slices were treated in a blocking buffer [5% normal goat serum in 0.3% PBS–Tween 20 (PBS-T)] for 45 min and incubated with primary antibody solution for 48 h. Slices were then washed and incubated for 2–3 h with a secondary antibody. EYFP fluorescence from ChR2$^+$ GCs was enhanced using a mouse anti-GFP (1:500; catalog #11814460, Sigma-Aldrich) and goat anti-mouse conjugated to Alexa Fluor 488 (1:500; catalog #A21121, Thermo Fisher Scientific) diluted in PBS-T. A mounting medium containing DAPI was used (VECTASHIELD, Vector Laboratories). The slide scanner was a Nanozoomer 2.0HT with a fluorescence imaging module (Hamamatsu Photonics) using a planar apochromatic 20 × objective with NA of 0.75 combined with an additional lens 1.75×, with a 2 × 2 binning leading to a final magnification of 20×. Virtual slides were acquired with a 3CCD camera with a time-delay and integration sensor. Fluorescent acquisitions were performed with a mercury lamp (LX2000 200W, Hamamatsu Photonics) and the set of filters adapted for GFP and DAPI fluorescence. An average of 10.1 ± 0.9 slices/mouse were analyzed in 10 mice. The analysis, area measurement, and counting of GFP$^+$ cells were performed manually with the software NDP View 2 (Hamamatsu Photonics).The percentage of ChR2$^+$ GCs was estimated by dividing the number of GFP$^+$ cells/mouse by the total number of GCs in the hippocampi of age-matched mice (Kempermann et al., 1997). The range of ChR2$^+$ GCs activated by light during *in vivo* experiments was estimated considering the geometrical properties of the light cone emitted through the optical fiber. The numerical aperture of the fiber (0.22) and the refraction index of the gray matter (1.36; Aravanis et al., 2007) allowed the calculation of the angle of divergence of the cone. Thus, we estimated that for a distance ranging from 200 to 400 μm (height of the cone) from the fiber tip we could find 4–31 cells. At these distances from the fiber tip, we had power attenuations (3 mW was the power measured at the fiber tip outside the brain) of 0.39 and 0.23, respectively (http://web.stanford.edu/group/dlab/cgi-bin/graph/chart.php).

To recover the morphology of neurons filled with biocytin during *in vivo* whole-cell patch-clamp recordings, brains were removed after the completion of electrophysiology experiments and were fixed for 1 week at 4°C in a solution containing 4% PFA in 1 × PBS, pH 7.4. Coronal slices (100 μm thick) were washed three times with 0.3% Triton X-100 in 1 × PBS (20 min each) and incubated overnight at 4°C in 1:1000 Alexa Fluor 488 or 555 streptavidin conjugated in the same solution. In between all experimental procedures, slices were washed with 1 × PBS. We successfully recovered the morphology of CA3 hippocampal neurons in 20 of 26 neurons. Immunofluorescence of mounted coverslips was acquired with a spinning disk microscope (model DMI6000, Leica Microsystems) equipped with a confocal Scanner Unit CSU-X1 (Yokogawa) using an HC PL Fluotar 10 × dry objective with NA of 0.3, an HCX PL Apo 40 × oil objective with NA of 1.25, an HCX PL Apo CS 63 × oil objective with NA of 1.4, and an HCX PL Apo 100 × oil objectives with NA 1.4, and an Evolve EMCCD camera (Photometrics) or an HQ2 CCD camera (Photometrics). The diode lasers used were at 408, 491, and 561 nm. The *z*-stacks were performed with a galvanometric stage (Leica Microsystems). The 37°C atmosphere was created with an incubator box and an air heating system (Life Imaging Services). This system was controlled by MetaMorph software (Molecular Devices). High-resolution stacks were generated using ImageJ software.

Drugs. The following drugs were used: CGP55845, gabazine (Tocris Bioscience). Aliquots of stock solutions were prepared and frozen at −20°C. All other chemicals were purchased from Sigma-Aldrich.

Statistical analysis. Values are given as the mean ± SEM of *n* experiments. Significance of differences was assessed by Student's paired or unpaired *t* test and ANOVA, as indicated. A Mann–Whitney test was used for comparison of two groups, and a Kruskal–Wallis test followed by a Dunn's multiple-comparison test for comparison was used for comparison of more than two groups. Within-cell comparisons were made with a Wilcoxon matched pairs test in raw non-normalized values between baseline values and values obtained after applying the stimulation protocol. Statistical differences were considered as significant at $p < 0.05$. Statistical analysis was performed with GraphPad Prism software.

Results

Light-induced short-term plasticity at mf–CA3 synapses in slices and *in vivo*

We delivered an adeno-associated viral vector encoding the ChR2 variant H134R-EYFP in the DG of POMC-Cre mice (Fig. 1*A*; Atasoy et al., 2008). Histological inspection revealed expression of EYFP in a restricted population of GCs over the entire width of the DG GC layer and not in other hippocampal cell types (Fig. 1*A*). We estimated that 4.5 ± 1.1% of the total number of DG GCs expressed ChR2-EYFP (see Materials and Methods). We then prepared slices to compare the intrinsic membrane properties of uninfected GCs (EYFP$^-$), GCs infected with a control EYFP virus (EYFP$^+$), and GCs infected with ChR2-EYFP

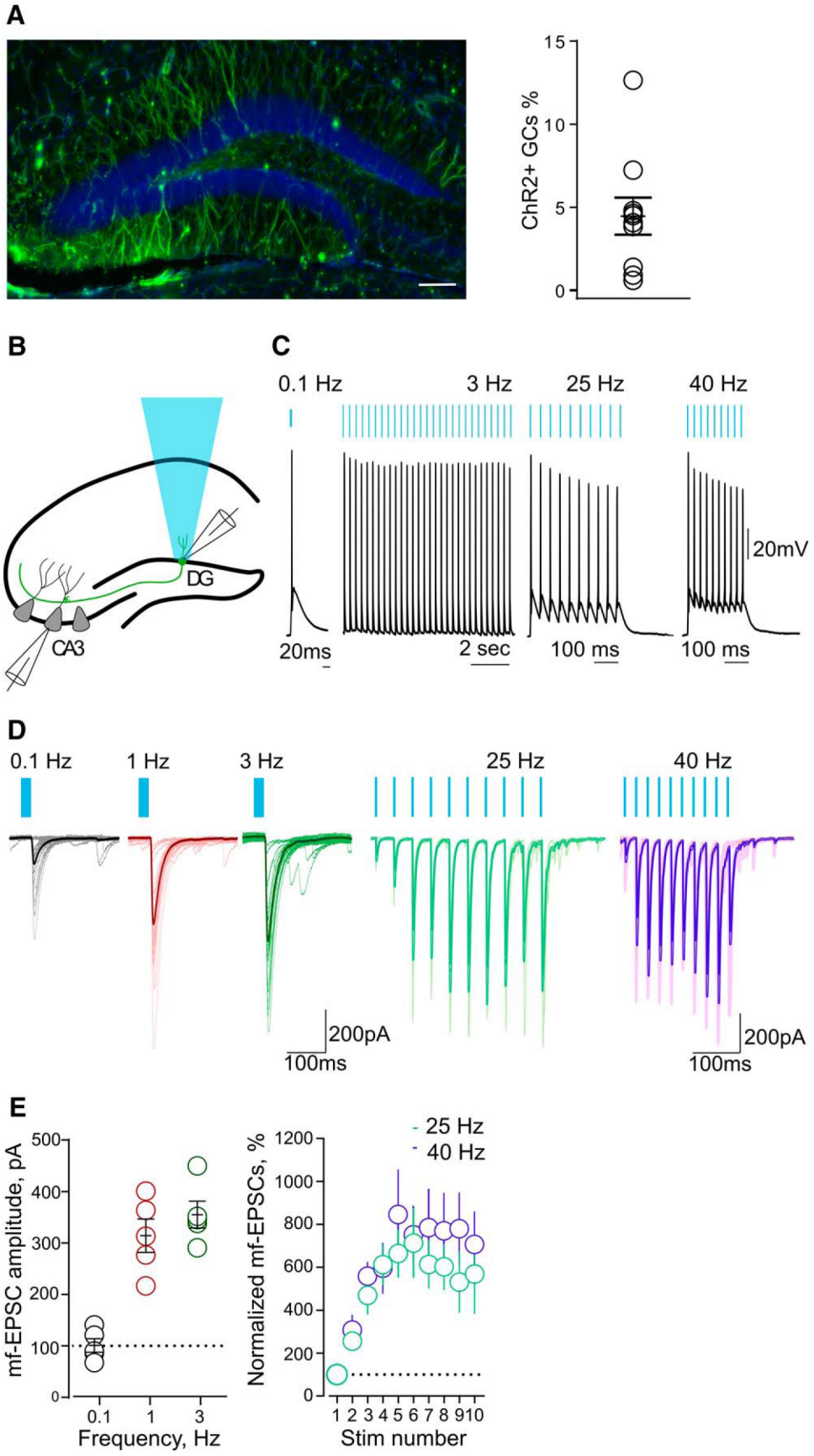

Figure 1. Light-induced short-term plasticity at mf–CA3 synapses in slices. ***A***, Confocal fluorescent image (left) illustrating ChR2-EYFP expression in GCs of the DG. Scale bar, 100 μm. On the right, a summary plot shows the percentage of GCs expressing ChR2-EYFP (right; $n = 10$ mice). ***B***, Schematic illustration of the hippocampus for experimental settings during optical stimulation of GCs in acute slices. ***C***, Current-clamp recordings showing DG cell firing in response to patterned blue light (0.1–40 Hz). Blue bars indicate light stimulation. (*Figure legend continues.*)

Table 1. Passive and active properties of POMC GCs

	EYFP $^-$	EYFP $^+$	ChR2–EYFP
RMP (mV)	71.6 ± 1.4 (15)	69.8 ± 1.7 (9)	62.4 ± 2.8 (9)*
Input resistance (MΩ)	584 ± 40 (14)	440 ± 52 (7)	503 ± 55 (8)
Spontaneous AP frequency (Hz)	0 (14)	0 (7)	0 (8)
AP voltage threshold (mV)	46.4 ± 0.7 (14)	47.4 ± 1.1 (11)	44.8 ± 1.3 mV (8)

Values are reported as the mean ± SEM; values in parentheses indicate the number of cells.
*Significance based on one-way ANOVA (see Materials and Methods).

(ChR2 $^+$ GCs; Table 1). No difference was observed among EYFP $^-$, EYFP $^+$, and ChR2 $^+$ GCs in input resistance. Resting membrane potential was similar in EYFP $^-$ and EYFP $^+$ GCs. ChR2 $^+$ GCs showed a more depolarized resting membrane potential in comparison with EYFP $^-$ GCs. However, in the absence of stimulation, GCs from both groups did not fire a single action potential in resting conditions, and we did not find any difference in the threshold for action potential generation during 1 s current pulses. These results strongly suggest that POMC GCs represent a subpopulation of GCs with electrophysiological properties of mature DG neurons (Schmidt-Hieber et al., 2004). Brief pulses (5 ms, 470 nm) of light at frequencies from 0.1 to 40 Hz reliably triggered single action potentials in ChR2 $^+$ GCs without any failures (Fig. 1*B*,*C*).

To examine whether classic synaptic properties of DG–CA3 connections can be elicited optogenetically, we combined light stimulation of GCs with electrophysiological recordings from single CA3 pyramidal neurons in slices. We then recorded EPSCs from CA3 PCs evoked by optogenetic stimulation of the soma of presynaptic GCs (Fig. 1*B*). At 0.1 Hz, mf-EPSCs had an average latency of 5.3 ± 0.8 ms ($n = 5$), an average amplitude of 101.0 ± 13.1 pA ($n = 5$), and an average percentage of failures of 18.0 ± 3.3% ($n = 5$). These values are in the range of *in vitro* measurements obtained with minimal electrical stimulation (Marchal and Mulle, 2004), suggesting that with this viral infection rate mf-EPSCs was evoked by light stimulation rather from one or a few GCs. Increasing the stimulation frequency from 0.1 to 1–3 Hz induced a significant facilitation of mf-EPSC amplitude ($p = 0.0082$, one-way ANOVA; Fig. 1*D*,*E*). Bursts of light stimulation consisting of short trains at 25 and 40 Hz also induced a robust increase in the amplitude of mf-CA3 EPSCs over the course of the train (25 Hz: $p = 0.0023$, one-way ANOVA; 40 Hz: $p = 0.033$; Fig. 1*D*,*E*). Hence, light activation of ChR2 $^+$ GCs faithfully evoked mf–CA3 synaptic responses over a wide range of frequencies, with properties of short-term synaptic plasticity comparable to those obtained with electrical stimulation in slice recordings (Nicoll and Schmitz, 2005).

As a first evaluation of synaptic properties of DG–CA3 connections *in vivo*, we recorded field postsynaptic potentials above the CA3 pyramidal layer (Fig. 2*A*–*C*). An optical fiber was placed above the GC layer of the DG in anesthetized mice to deliver light stimulation (see Materials and Methods; Fig. 2*A*). Light was delivered at low frequency (0.05 Hz) to measure basal transmission, and then switched to higher frequencies (1, 3, and 10 Hz; Fig. 2*B*,*D*). This protocol produced a marked potentiation of fEPSPs, the early excitatory component of the response (percentage of fEPSP slopes vs baseline: at 0.05 Hz, 1 Hz: 107 ± 10%; at 3 Hz: 280 ± 30%; at 10 Hz: 480 ± 90%; $n = 8$, $p = 0.0061$, one-way ANOVA). Similarly, a gradual and robust facilitation of fEPSPs was observed when light stimulation was delivered in trains [percentage of fEPSP slope: 10th vs 1st stimulation: 20 Hz, 501 ± 80 ($n = 14$, $p = 0.0001$); 10th vs 1st stimulation: 40 Hz (470 ± 90, $n = 12$, $p = 0.0005$, Wilcoxon matched-pairs test); Fig. 2*C*,*D*]. These results indicate that both tonic and train firing patterns result in facilitation of mf–CA3 transmission *in vivo* as described previously with bulk electrical stimulation protocols (Klausnitzer and Manahan-Vaughan, 2008; Hagena and Manahan-Vaughan, 2010).

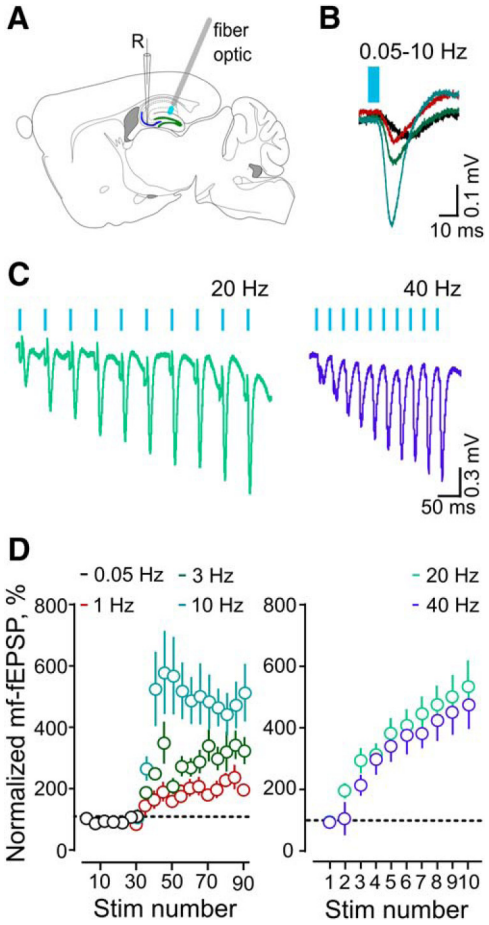

Figure 2. *In vivo* characterization of mf–CA3 synaptic responses. ***A***, Scheme showing the placement of fiber-optic and recording electrodes (R) for fEPSP. ***B***, Representative fEPSP average traces obtained with optical stimulation at 0.05–10 Hz ($n = 8$). ***C***, Representative fEPSP average traces obtained with five trains of optical stimulation at 20 Hz ($n = 14$) and 40 Hz ($n = 12$). ***D***, Averaged time courses for the normalized fEPSPs slopes shown in ***B*** (left) and ***C*** (right).

Light stimulation of GCs induces a slow hyperpolarization in CA3 PCs *in vivo*

To study the properties of synaptic transmission at DG–CA3 connections at a single-cell level *in vivo*, we turned to patch-clamp recordings. We first investigated the electrophysiological properties of single GCs and CA3 PCs *in vivo* (Fig. 3), which were identified morphologically following the recovery of biocytin-filled cells (Fig. 3*A*,*C*). In the absence of stimulation, GCs showed hyperpolarized resting membrane potentials alternating with frequent periods of depolarization and did not fire spontaneously (Fig. 3*A*,*B*), which is in agreement with recent studies *in vivo* (Pernía-Andrade and Jonas, 2014; Kowalski et al., 2016). Spike

←

(*Figure legend continued.*) ***D***, Representative traces of 30 consecutive mf–EPSCs evoked at 0.1–3 Hz. Averaged traces are superimposed (left). Representative traces of mf–EPSCs evoked with trains of light stimulation at 25 and 40 Hz. Averaged traces are superimposed (right). ***E***, Summary graph of averaged mf-EPSCs amplitude ($n = 5$) evoked at 0.1–3 Hz (left). Averaged time courses ($n = 5$) for the normalized mf-EPSCs amplitude evoked at 25 and 40 Hz (right).

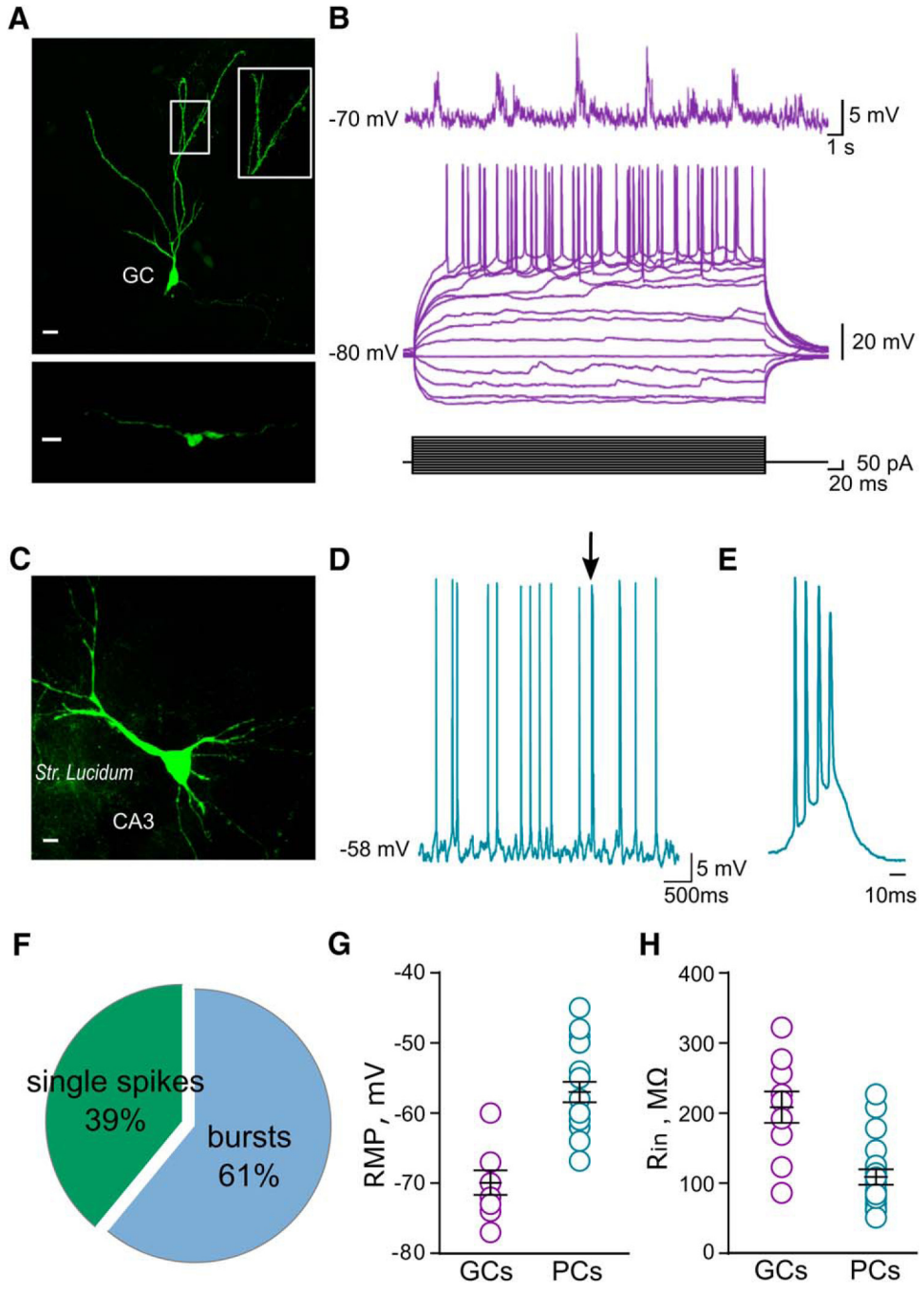

Figure 3. Electrophysiological characterization of GCs and CA3 PCs *in vivo*. ***A***, Confocal fluorescent image of a DG cell filled with biocytin during whole-cell recording and visualized by *post hoc* labeling with Alexa Fluor 488. Scale bar, 10 μm. Dendritic spines from the same cells are plotted at higher magnification. Inset scale bar, 20 μm. The bottom part shows a mossy fiber bouton from the same DG cell in stratum lucidum. Scale bar, 5 μm. ***B***, Example trace of a current-clamp recording from a DG cell showing lack of spontaneous firing, membrane potential oscillations (top), and subthreshold and suprathreshold responses to injected current pulses (bottom). ***C***, Confocal fluorescent image of a CA3 PC filled with biocytin during whole-cell recording and visualized by *post hoc* labeling with Alexa Fluor 488. Scale bar, 10 μm. ***D***, Example trace of a current-clamp recording from a CA3 PC showing spontaneous single and bursts of action potentials (arrow). ***E***, Example of burst of action potentials obtained from traces shown in ***D***. ***F***, Pie chart showing the proportion of single action potentials vs bursts in CA3 PCs. ***G***, Scatter plot graph summarizing resting membrane potential (left) and (***H***) input resistance (right) of GCs ($n = 12$) and CA3 PCs ($n = 20$).

discharge could, however, be triggered by positive current steps (Fig. 3*B*). CA3 PCs were characterized by low spontaneous firing frequency (2 ± 0.38 Hz; $n = 11$), which consisted of both single spikes and bursts of action potentials (single APs, 38.9 ± 9.4%; bursts, 61.1 ± 9.4%; $n = 11$; Fig. 3*D–F*). CA3 PCs displayed a more depolarized membrane potential compared with GCs [−57 ± 1.3 mV ($n = 20$) vs −70.3 ± 1.6 mV ($n = 9$), respectively] and lower input resistance [108.8 ± 10.9 MΩ ($n = 20$) vs 209 ± 22 MΩ ($n = 9$); Fig. 3*G*,*H*].

We then characterized mf–CA3 synaptic responses *in vivo* from CA3 PCs in the patch-clamp, current-clamp configuration (Fig. 4). In addition to direct excitation of CA3 PCs, GCs also provide excitatory synaptic inputs to CA3 INs via filopodia extensions of the mf bouton and en passant synapses (Fig. 4*A*). Accordingly, light stimulation of DG cells generated a biphasic synaptic response in CA3 PCs, which was shaped by stimulation frequency (Fig. 4*C*,*D*). At low stimulation frequency (0.05 Hz), mf–CA3 synaptic responses consisted pre-

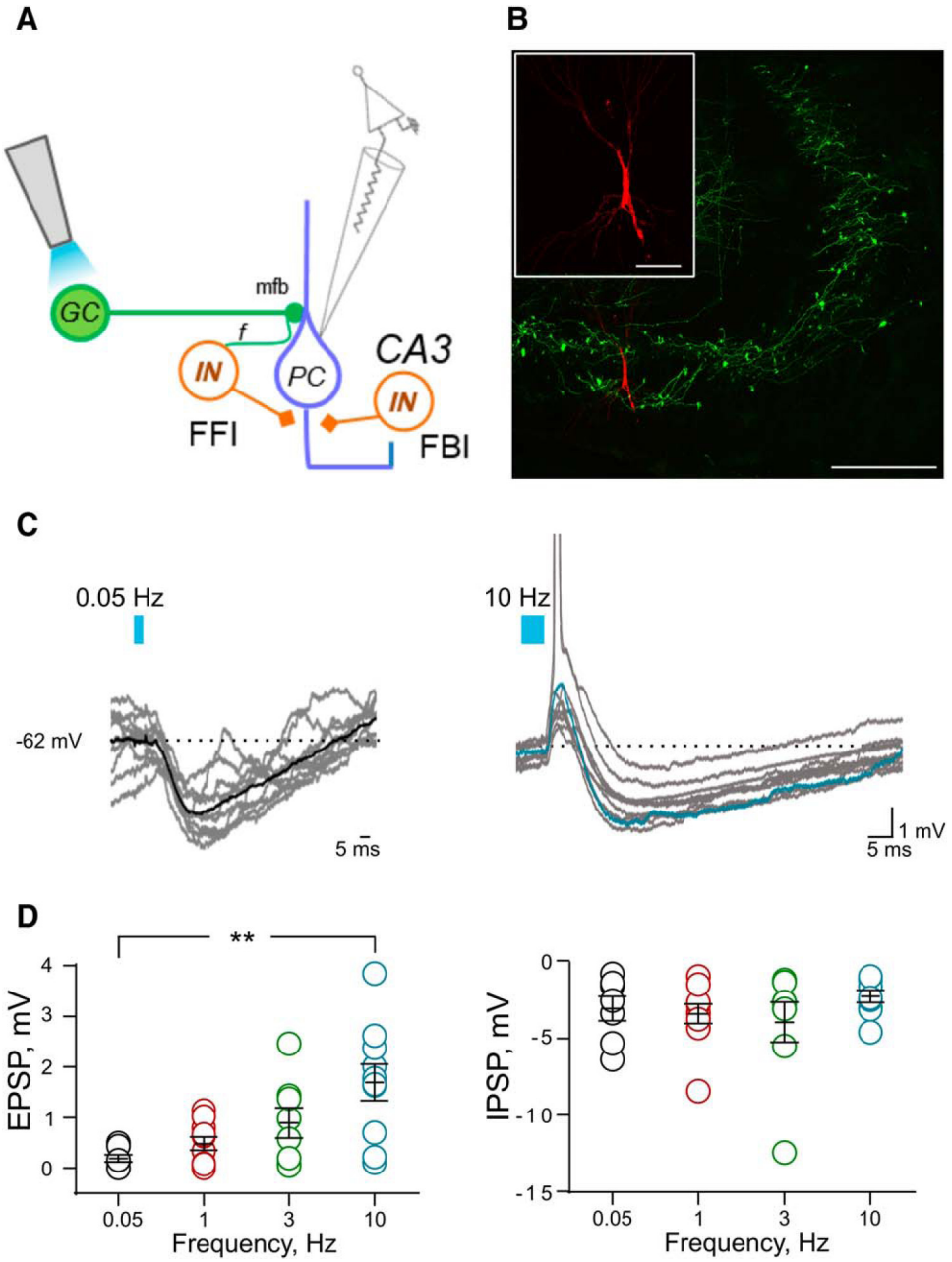

Figure 4. Light stimulation of GCs induces a slow hyperpolarization in CA3 PCs *in vivo*. ***A***, Schematic representation of the hippocampal CA3 microcircuit, showing the experimental configuration for light stimulation and recording site. ***B***, Confocal fluorescent image showing ChR2 expression in mfs in the stratum lucidum (EYFP) and a CA3 PC filled with biocytin in whole-cell recording (Alexa Fluor 555). Scale bar, 100 μm. The inset shows the same CA3 neuron at higher magnification. Scale bar, 20 μm. ***C***, Synaptic potentials evoked with increasing frequencies of optical stimulation of GCs. Representative traces of 10 consecutive responses evoked at 0.05 Hz (left) and 10 Hz (right) are shown (spikes appear truncated). Averaged traces obtained from subthreshold synaptic responses are superimposed. ***D***, Scatter plot showing frequency-dependent facilitation of light-evoked mf–EPSP amplitude (left) and stable light-evoked mf–IPSP amplitude (right).

dominantly of an IPSP, and in most instances EPSPs could not be detected (Fig. 4*C*). The mf–CA3 EPSPs became apparent upon increasing the frequency of stimulation, which produced a gradual facilitation of mf–CA3 EPSP amplitudes (0.05 Hz, 0.18 ± 0.07 mV; 1 Hz, 0.48 ± 0.13 mV; 3 Hz, 0.89 ± 0.29 mV; 10 Hz, 1.69 ± 0.36 mV; n = 7–10; Fig. 4*C*,*D*). Increasing stimulation frequency resulted in an increase in the probability of spike discharge (Fig. 4 *C*; 0.05 vs 10 Hz; $^{**}p < 0.0075$, Dunn's multiple-comparison test). In contrast with the excitatory component of the response, the IPSP that followed mf–CA3 EPSPs were not significantly affected by changes in frequencies (0.05 Hz, −2.98 ± 0.79 mV; 1 Hz, −3.32 ± 0.64 mV; 3 Hz, −3.87 ± 1.3 mV; 10 Hz, −2.19 ± 0.39 mV; n = 7–10; Fig. 4*D*). The inhibitory response was characterized by its long duration (at 1 Hz, 119.1 ± 14.6 ms; n = 10). The duration of the inhibitory response did not significantly differ when changing the frequency of light stimulation [0.05 Hz, 105.8 ± 14.9 ms; 1 Hz, 119.1 ± 14.6 ms; 3 Hz, 115.3 ± 12.7 ms; 10 Hz, 88.7 ± 4.8 ms (p = 0.4732, one-way ANOVA)]. This is a first description of subthreshold synaptic transmission at mf–CA3 synapses *in vivo*. It clearly indicates that GCs elicit synaptic inhibition which lasts on the order of 100 ms whatever the presynaptic stimulation rate (within the 0.05–10 Hz range). In contrast, increased stimulation frequency results in

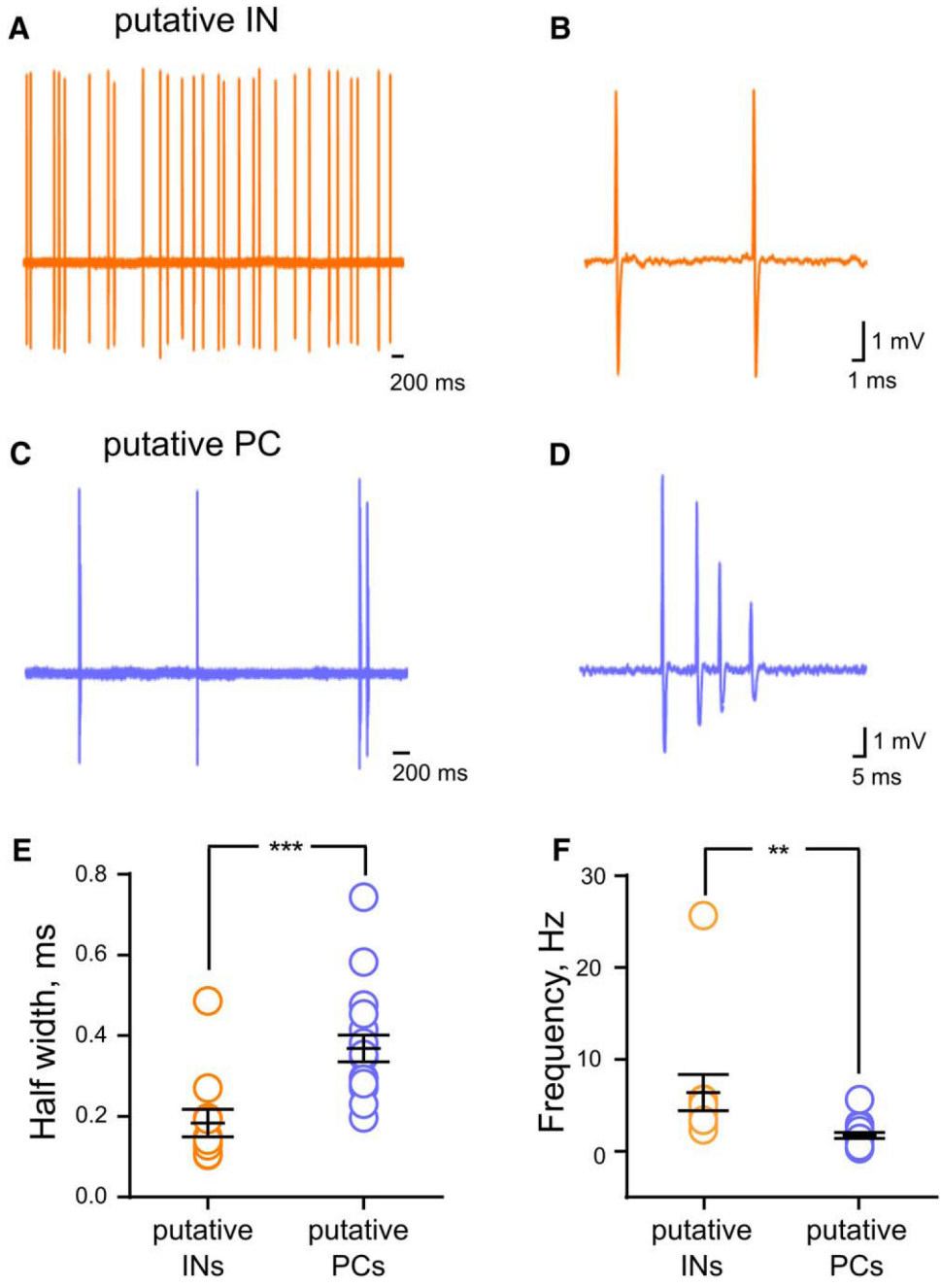

Figure 5. Characterization of CA3 neurons firing *in vivo* with juxtacellular recordings. ***A***, Representative high-pass-filtered (100 Hz) spike traces recorded from a putative CA3 IN. ***B***, Trace illustrating the action potential shape from the same cell in ***A***. ***C***, Representative high-pass-filtered (100 Hz) spike traces recorded from a putative CA3 PC. ***D***, Trace showing a typical burst of action potential from the same cell in ***C***. ***E***, Scatter plot graph showing average half-width of the action potentials recorded from putative CA3 INs (orange) and putative CA3 PCs (violet). ***F***, Scatter plot graph showing the average spontaneous frequency of action potentials recorded from putative INs (orange, $n = 11$) and putative PCs (violet, $n = 17$).

short-term facilitation of mf–CA3 EPSPs, hence in gradual amplification of excitation with regard to inhibition.

Activation of the local feedforward circuit controls CA3 excitability *in vivo*

We further investigated the role of local INs in shaping the spiking output of CA3 neurons. In juxtacellular recordings, two populations of neurons could clearly be distinguished on the basis of spontaneous firing frequency, firing mode, and spike waveform, which corresponded to populations of putative INs and putative PCs (Csicsvari et al., 1999). CA3 INs preferentially fired single action potentials (Fig. 5*A*,*B*), whereas CA3 PCs fired in a mixed mode with single action potentials and short bursts (Fig. 5*C*,*D*). CA3 INs had a significantly higher mean firing rate [INs, 6.4 ± 2 ($n = 11$); PCs, 1.73 ± 0.3 Hz ($n = 17$); $^{**}p = 0.007$, unpaired *t* test] and narrower spikes [INs, 0.18 ± 0.03 ms half-width ($n = 11$); PCs, 0.37 ± 0.03 ms half-width ($n = 17$); $^{***}p = 0.001$, unpaired *t* test; Fig. 5*E*,*F*]. No difference was observed in the half-width and spontaneous firing frequency of CA3 PCs recorded in isoflurane anesthetized mice and those recorded under ketamine/xylazine anesthesia [half-width: 0.37 ± 0.03 $n = 17$ vs 0.4 ± 0.02 ($n = 8$; $p = 0.47$, unpaired *t* test); frequency: 4.16 ± 0.6 Hz ($n = 17$) vs 3.81 ± 0.9 ($n = 8$, $p = 0.77$, unpaired *t* test]. We then examined the impact of the optical stimulation of GCs on

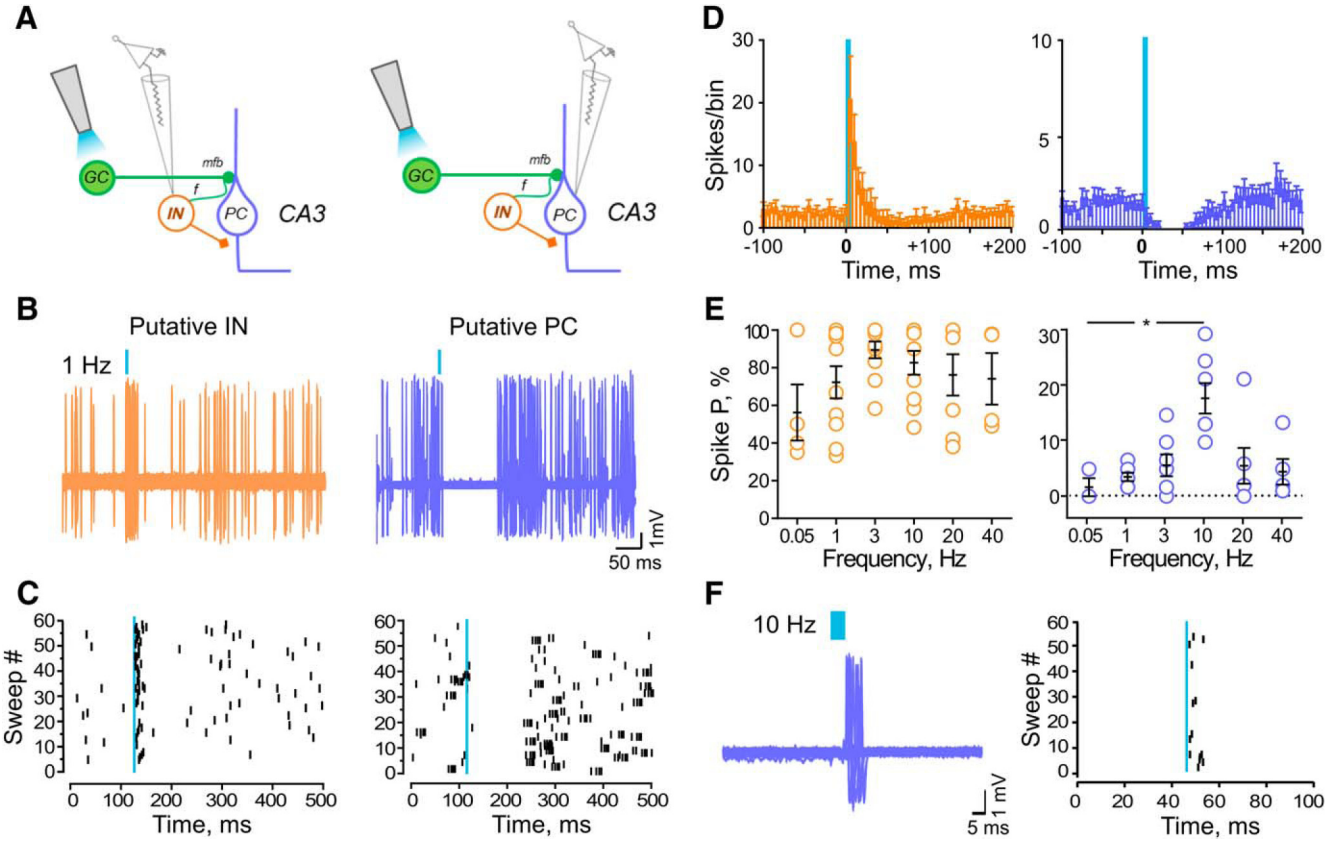

Figure 6. DG cell stimulation reliably activates INs driving feedforward inhibition in CA3 PCs *in vivo*. ***A***, Schematic representation of the hippocampal CA3 microcircuit, showing fiber-optic placement for light stimulation of presynaptic GCs and postsynaptic recording site of CA3 INs (left) or CA3 PCs (right). ***B***, Light stimulation of GCs at 1 Hz reliably discharges putative CA3 INs (left) and induces firing inhibition in CA3 PCs (right). ***C***, Raster plot obtained from the representative traces shown in ***B***. ***D***, Cumulative perievent time histogram showing the average number of spikes per bin (bin size, 5 ms) in CA3 INs (left, $n = 10$) and PCs (right, $n = 14$) before and after 1 Hz light stimulation of GCs. ***E***, Spike probability (P), measured within 30 ms interval from the beginning of the light pulse (dashed line) at different frequencies. Scatter plot graph (left) showing a significant increase in spike probability in INs ($n = 10$). The spike probability of the INs is not affected by the frequency of stimulation. Scatter plot graph (right) showing a significant increase in spike probability in CA3 PCs ($n = 7$) following 10 Hz stimulation. ***F***, The 10 Hz light stimulation of GCs reliably discharges CA3 PCs (left). Raster plot obtained from the representative traces shown in ***F***.

the firing of putative CA3 INs and PCs (Fig. 6*A*). In CA3 PCs, light stimulation at 1 Hz induced a strong inhibition of spontaneous firing (Fig. 6*B–D*). A subpopulation of CA3 PCs was not affected by light stimulation (data not shown), which is in agreement with the sparse anatomical connections of mf–CA3 PCs (Henze et al., 2000; Nicoll and Schmitz, 2005; Evstratova and Tóth, 2014) and the low percentage of GC cells expressing ChR2 (Fig. 1*A*). Repetitive pulses of light at 1 Hz reliably discharged CA3 INs, and 6 of 10 CA3 INs consistently showed multiple spikes; increasing the frequency of stimulation did not change the spike probability (Fig. 6*E*). In contrast, stimulation at 10 Hz increased the probability of action potential discharge in 7 of 14 CA3 PCs (Fig. 6*E*,*F*). The spike probability response in CA3 PCs was significantly different between 0.05 and 10 Hz [0.05 Hz, 1.7 ± 1.7% ($n = 4$); 1 Hz, 3.6 ± 0.8% ($n = 7$); 3 Hz, 5.7 ± 2% ($n = 7$); 10 Hz, 18.1 ± 2.8% ($n = 7$); 20 Hz, 5.6 ± 3.3% ($n = 5$); 40 Hz, 4.5 ± 2.4% ($n = 6$); $^{*}p < 0.014$, one-way ANOVA; Fig. 6*E*]. Increasing presynaptic stimulation frequency also resulted in a significantly shorter duration of light-driven inhibition (1 Hz, 98.2 ± 11 ms; 10 Hz, 65.4 ± 5.6 ms; $n = 14$; $^{**}p = 0.004$, paired *t* test). Both populations of neurons, when firing, discharged with a fixed latency [CA3 PCs, 6.8 ± 1.6 ms ($n = 7$); CA3 INs, 7.2 ± 0.9 ms ($n = 12$)], thus providing evidence for monosynaptic connections between GCs and their postsynaptic targets.

Involvement of both $GABA_A$ and $GABA_B$ receptors in feedforward inhibition *in vivo*

The results described above demonstrate that activation of a feedforward inhibitory circuit provides a robust inhibition, which tightly controls spike transmission of DG–CA3 PCs *in vivo*. DG-driven feedforward inhibition characterized in slices triggers a disynaptic IPSC in CA3 PCs carried by $GABA_A$ receptors (Torborg et al., 2010). We thus checked the involvement of $GABA_A$ receptors in the inhibition of CA3 PCs firing in response to optical stimulation of GCs *in vivo* (Fig. 7). Local application of the specific $GABA_A$ antagonist gabazine (500 μM) significantly increased the firing probability in response to GCs stimulation at 1 Hz (control, 2.7 ± 0.7%; gabazine, 34.8 ± 4%; $n = 8$; $^{**}p = 0.008$, Wilcoxon matched pairs signed rank test; Fig. 7*A*,*B*). In the presence of gabazine, all CA3 PCs discharged single spikes or bursts of action potentials following light stimulation.

These results indicate that the initial phase of feedforward inhibition is mediated by the activation of $GABA_A$ receptors, which curtail phase-locked spike transfer. However, gabazine did not affect the duration of inhibition induced by optical stimulation of GCs (control, 78 ± 4 ms; gabazine, 105 ± 14 ms; $n = 8$; $p = 0.09$, Wilcoxon matched-pairs signed rank test; Fig. 7*A*,*B*), which is consistent with the observation that the duration of DG-driven inhibition likely exceeds typical IPSCs generated by

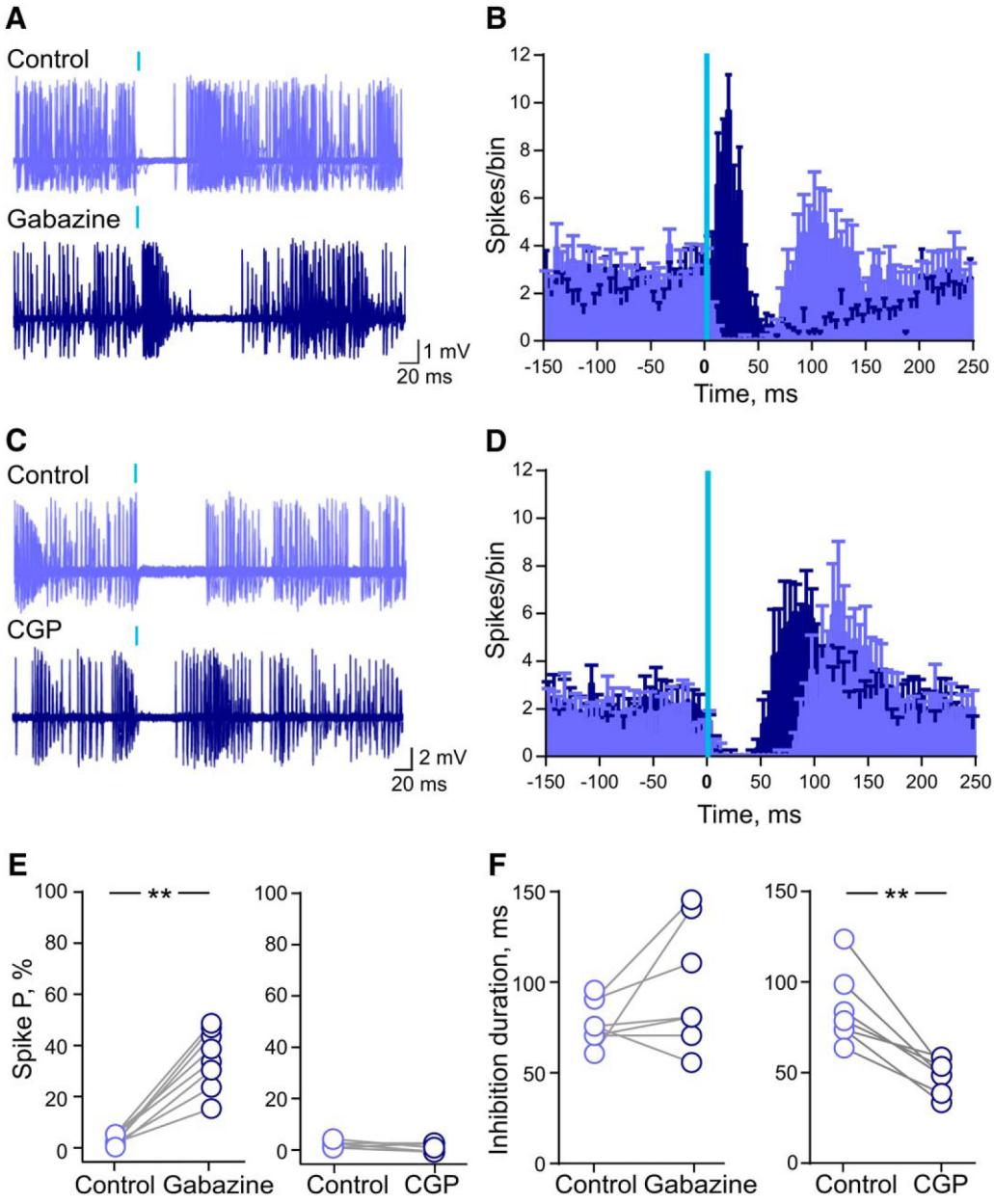

Figure 7. Involvement of both $GABA_A$ and $GABA_B$ receptors in feedforward inhibition *in vivo*. ***A***, Superimposed traces obtained from a putative CA3 PC (up) showing light-induced firing inhibition in a control condition and after local application of gabazine 500 μM (bottom). ***B***, Cumulative perievent time histogram showing the average number of spikes per bin (bin size, 5 ms) in the control condition (violet) and after gabazine application (blue, $n = 8$). ***C***, Superimposed traces obtained from a putative CA3 PC (up) showing light-induced firing inhibition in control condition and after local application of CGP55845 500 μM (bottom). ***D***, Cumulative perievent time histogram showing the average number of spikes per bin (bin size, 5 ms) in the control condition (violet) and after CGP55845 application (blue, $n = 7$). ***E***, Scatter plot graph showing changes in mf-driven spike probability after gabazine (left, $n = 8$) and CGP55845 (right, $n = 7$) application. ***F***, Scatter plot graph showing the duration of inhibition after gabazine (left, $n = 8$) and CGP55845 (right, $n = 7$) application.

$GABA_A$ receptors (on the order of 30 ms (Torborg et al., 2010). We thus examined the involvement of $GABA_B$ receptors in DG-driven feedforward inhibition of spike transfer in CA3 PCs. Local application of the specific $GABA_B$ antagonist CGP55845 (500 μM) significantly reduced the slow inhibition in CA3 PCs during 1 Hz stimulation (control, 86 ± 7.6 ms; CGP55845, 49 ± 3.3 ms; $n = 7$; $^{**}p = 0.008$, Wilcoxon matched pairs signed rank test; Fig. 7*C–F*). This strongly suggests that the late phase of the IPSP recorded in the current-clamp mode is mediated by the activation of $GABA_B$ receptors. CGP55845 application did not affect spontaneous firing or the initial spike discharge (within 30 ms from the beginning of the light pulse; control, 2.6 ± 0.5%; CGP55845, 1.7 ± 0.6%; $n = 7$; $p = 0.12$, Wilcoxon matched pairs signed rank test) evoked by light stimulation of DG GCs (Fig. 7*E*). Altogether, our data demonstrate how the intact CA3 circuit feedforward inhibition driven by GCs triggers both a rapid inhibition mediated by $GABA_A$ receptors and a slow inhibition mediated by $GABA_B$ receptors, which sets the temporal rules for spike transfer at DG–CA3 connections.

Discussion

Our work extends from the extensive studies of mf–CA3 synapses in rodent slice recordings (Henze et al., 2000; Nicoll and Schmitz, 2005; McBain, 2008; Sachidhanandam et al., 2009) to the intact brain *in vivo* and directly characterizes synaptic transmission at DG–CA3 connections. In slices, the amplitude of mf synaptic currents in CA3

PCs is highly conditioned by the pattern of presynaptic activity (Henze et al., 2002; Nicoll and Schmitz, 2005). At a low frequency of presynaptic GC activity (<0.1 Hz), mf-EPSPs do not trigger action potential discharge because of a very low release probability at individual release sites ($p < 0.01$; Nicoll and Schmitz, 2005; Lanore et al., 2012; Evstratova and Tóth, 2014; Cherubini and Miles, 2015). However, postsynaptic action potentials are triggered in slice recordings with repeated presynaptic activity (Henze et al., 2002; Klausnitzer and Manahan-Vaughan, 2008; Sachidhanandam et al., 2009). This is a consequence of the wide dynamic range of presynaptic short-term plasticity upon repeated stimulation (Salin et al., 1996; Sachidhanandam et al., 2009) combined with a large number of release sites, a large vesicle pool size, and multivesicular release (Margrie et al., 2002; Hallermann et al., 2003; Lee et al., 2009; Chamberland et al., 2014). To date, very little is known about the properties of short-term plasticity at mf–CA3 synapses *in vivo*. Frequency facilitation, a tonic form of plasticity, leads to increased magnitude of fEPSPs in CA3 elicited by low-frequency electrical stimulation of the DG (1–2 Hz) in freely behaving rats (Georges and Aston-Jones, 2002; Klausnitzer and Manahan-Vaughan, 2008). However, in these conditions, paired-pulse facilitation of fEPSPs is weak and is observed only for an interstimulus interval of 50 ms (Atasoy et al., 2008; Hagena and Manahan-Vaughan, 2010), in stark contrast with slice recordings (Schmidt-Hieber et al., 2004; Nicoll and Schmitz, 2005), even in fully developed hippocampus, such as what is described here (mice >6 weeks old). Frequency facilitation of fEPSPs evoked by light activation of DG cells was apparent *in vivo* when shifting the frequency from 0.05 to 1 Hz, although it appeared somewhat attenuated compared with slice recordings, in which a fourfold fivefold amplitude increase can be observed for the same frequency range. The lower extracellular calcium concentration *in vivo* may contribute to the difference in release probability and short-term plasticity (Lorteije et al., 2009). Strong facilitation of information transfer between the DG and CA3 PCs occurs *in vivo* only with high frequencies of presynaptic GCs activity (Henze et al., 2002), but the underlying synaptic mechanisms have not been investigated yet.

Here we characterized the properties of mf–CA3 synaptic transmission using whole-cell current-clamp recordings of CA3 PCs *in vivo*. Feedforward inhibition appears to play a major role in controlling information transfer at DG–CA3 connections *in vivo*. Optical stimulation of GCs triggers a robust slow inhibition (in the 100 ms range) in single CA3 PCs recorded in the current–clamp mode. At a low frequency of GC activity (1–3 Hz), the mf–CA3 EPSP is either absent or blunted by disynaptic inhibition. The gradual increase in the frequency of stimulation induces a significant facilitation of mf–CA3 EPSPs, with the amplitude and duration of IPSPs remaining unchanged. Accordingly, juxtacellular recordings from putative CA3 INs indicate that spike transfer at connections between the DG and CA3 INs is already very efficient at low presynaptic stimulation frequency and appears insensitive to increased frequency of GCs activity over a wide range, from 0.05 to 40 Hz. Thus, short-term facilitation of mf–CA3 PC EPSPs combined with the stable discharge of CA3–IN synapses leads to a progressive increase in the excitation/inhibition balance. We observed optimal spike transfer at mf–CA3 PC synapses with a frequency of stimulation of 10 Hz. This can be explained by the ~100-ms-long inhibition observed in CA3 PCs following a single stimulation of GCs. Inhibition during this time window likely prevents spike discharge for intervals between presynaptic spikes of <100 ms (e.g., at 20 and 40 Hz) even though mf–CA3 EPSPs are facilitated by short-term plasticity. Previous work has shown that the probability of spike transfer at mf–CA3 synapses steadily increases with frequency from 10 to 100 Hz (Henze et al., 2002). Our results differ somewhat from this previous study, although the reliability of optogenetics for precisely triggering action potentials above frequencies of 40 Hz prevented the testing of the same range of frequencies. In our experimental conditions, spike transfer at mf–CA3 IN synapses is very efficient, and the slow mf-driven inhibition induced in CA3 PCs is consistent with a refractory period for spike transfer corresponding to the 100 ms inhibition following DG stimulation.

Optogenetic stimulation of DG cells represents a clear advantage over bulk electrical stimulation in terms of cellular specificity. However, optogenetic stimulation does not avoid activating several presynaptic neurons in a time-locked manner, a situation that may not correspond to the physiological firing activity of DG cells. It was thus important to estimate the number of GCs that could be activated simultaneously by light. In the POMC-Cre mouse line used here, Cre is expressed in only <15–20% of DG GCs (E. Normand, unpublished observations). We directly estimated the percentage of $ChR2^+$ GCs to 4.5% of the total of DG cells. Our optical fiber (200 μm in diameter) positioned ~200 μm above the DG cell layer generated a light cone of 0.001–0.0076 mm^3 at 200 μm (GC dendritic layer) to 400 μm (GC somatic layer) from the fiber tip. This represents an estimated 4–31 DG GCs that can possibly be activated by a pulse of light (see Materials and Methods). Our experimental conditions to study the impact of DG GCs firing onto the CA3 microcircuit are thus compatible with the sparse action potential discharges of GCs observed in awake mice (Jung and McNaughton, 1993; Pernía-Andrade and Jonas, 2014). The robust inhibition triggered by light stimulation of DG GCs is likely attributed to feedforward inhibition (the same mf making synapses onto a given CA3 PC and onto CA3 INs that directly inhibit this same CA3 PC (Mori et al., 2007). Although we provide evidence that light activates only a limited number of DG GCs simultaneously in our experimental conditions, this potentially differs from previous experiments in organotypic cultures (Mori et al., 2004) and *in vivo* (Henze et al., 2002) in which a single presynaptic DG GC was activated. Therefore, we cannot exclude that the 100 ms time window of inhibition and the underlying $GABA_B$ receptor activation observed may be explained by the simultaneous activation of several mfs. Indeed, light stimulation of DG GCs may also activate CA3 INs, which then synapse onto a CA3 PC not being contacted by the same mf (a form of lateral inhibition).

Among the range of frequencies tested in our conditions, 10 Hz seems to be the optimized frequency of DG cell activity for spike transmission at DG–CA3 connections. Hence, our data suggest that EC incoming inputs to DG in the theta frequency range would be faithfully transmitted to CA3. It would be interesting to relate the temporal rule for spike transfer to the natural activity of DG cells during behavior. Future work should define the properties of spike transfer in awake mice, since anesthesia likely affects synaptic transmission, the duration of the feedforward inhibition, and spiking activity. It should be mentioned, however, that the spontaneous firing frequency reported here under isoflurane as well as ketamine/xylazine anesthesia is comparable to that reported with urethane anesthesia (Henze et al., 2002). Moreover, similar results for spike transfer in juxtacellular recordings of CA3 PCs were obtained under ketamine/xylazine anesthesia (data not shown). The slow inhibition (up to 100 ms) is thus a key parameter for defining the temporal rule for spike transfer at mf–CA3 PCs synapses. We found that this depended on the activation of $GABA_B$ receptors that likely trigger the slow IPSP recorded in CA3 PCs. Interestingly, a single pulse of light triggered in the DG is capable of inducing this long-lasting inhibition in CA3 PCs even at low frequency. In the neocortex and CA1 hippocampal region, single action potentials in neurogliaform cells

elicit slow inhibition in pyramidal neurons by the activation of $GABA_B$ receptors through their extremely dense axonal cloud (Tamás et al., 2003; Price et al., 2008). Of the four distinct GABAergic cell types contacted by mfs in CA3, ivy cells, which belong to the family of neurogliaform cells (Szabadics and Soltesz, 2009), appear as potential candidates for the extended duration of feedforward inhibition through $GABA_B$ activation, although other GABAergic inputs could also contribute (Degro et al., 2015).

In conclusion, the efficacy of spike transfer at DG–CA3 connections *in vivo* highly depends on a strictly timed balance between the direct excitation of CA3 PCs, which shows short-term facilitation, and robust and stable feedforward inhibition composed of a fast and a slow inhibitory component. Future work should evaluate the modulation of the excitation/inhibition balance in awake behaving conditions, especially in relation to oscillations.

References

Aravanis AM, Wang LP, Zhang F, Meltzer LA, Mogri MZ, Schneider MB, Deisseroth K (2007) An optical neural interface: in vivo control of rodent motor cortex with integrated fiberoptic and optogenetic technology. J Neural Eng 4:S143–S156. CrossRef Medline

Atasoy D, Aponte Y, Su HH, Sternson SM (2008) A FLEX switch targets channelrhodopsin-2 to multiple cell types for imaging and long-range circuit mapping. J Neurosci 28:7025–7030. CrossRef Medline

Chadderton P, Margrie TW, Häusser M (2004) Integration of quanta in cerebellar granule cells during sensory processing. Nature 428:856–860. CrossRef Medline

Chamberland S, Evstratova A, Tóth K (2014) Interplay between synchronization of multivesicular release and recruitment of additional release sites support short-term facilitation at hippocampal mossy fiber to CA3 pyramidal cells synapses. J Neurosci 34:11032–11047. CrossRef Medline

Cherubini E, Miles R (2015) The CA3 region of the hippocampus: how is it? What is it for? How does it do it? Front Cell Neurosci 9:19. CrossRef Medline

Chicurel ME, Harris KM (1992) Three-dimensional analysis of the structure and composition of CA3 branched dendritic spines and their synaptic relationships with mossy fiber boutons in the rat hippocampus. J Comp Neurol 325:169–182. CrossRef Medline

Csicsvari J, Hirase H, Czurkó A, Mamiya A, Buzsáki G (1999) Fast network oscillations in the hippocampal CA1 region of the behaving rat. J Neurosci 19:RC20. Medline

Degro CE, Kulik A, Booker SA, Vida I (2015) Compartmental distribution of GABAB receptor-mediated currents along the somatodendritic axis of hippocampal principal cells. Front Synaptic Neurosci 7:6. CrossRef Medline

Evstratova A, Tóth K (2014) Information processing and synaptic plasticity at hippocampal mossy fiber terminals. Front Cell Neurosci 8:28. CrossRef Medline

Gao X, Arlotta P, Macklis JD, Chen J (2007) Conditional knockout of catenin in postnatal-born dentate gyrus granule neurons results in dendritic malformation. J Neurosci 27:14317–14325. CrossRef Medline

Georges F, Aston-Jones G (2002) Activation of ventral tegmental area cells by the bed nucleus of the stria terminalis: a novel excitatory amino acid input to midbrain dopamine neurons. J Neurosci 22:5173–5187. Medline

Guzowski JF, Knierim JJ, Moser EI (2004) Ensemble dynamics of hippocampal regions ca3 and CA1. Neuron 44:581–584. CrossRef Medline

Hagena H, Manahan-Vaughan D (2010) Frequency facilitation at mossy fiber-CA3 synapses of freely behaving rats contributes to the induction of persistent LTD via an adenosine-A1 receptor-regulated mechanism. Cereb Cortex 20:1121–1130. CrossRef Medline

Hallermann S, Pawlu C, Jonas P, Heckmann M (2003) A large pool of releasable vesicles in a cortical glutamatergic synapse. Proc Natl Acad Sci U S A 100:8975–8980. CrossRef Medline

Henze DA, Urban NN, Barrionuevo G (2000) The multifarious hippocampal mossy fiber pathway: a review. Neuroscience 98:407–427. CrossRef Medline

Henze DA, Wittner L, Buzsáki G (2002) Single granule cells reliably discharge targets in the hippocampal CA3 network in vivo. Nat Neurosci 5:790–795. CrossRef Medline

Jung MW, McNaughton BL (1993) Spatial selectivity of unit activity in the hippocampal granular layer. Hippocampus 3:165–182. CrossRef Medline

Kempermann G, Kuhn HG, Gage FH (1997) More hippocampal neurons in adult mice living in an enriched environment. Nature 386:493–495. CrossRef Medline

Kesner RP, Rolls ET (2015) A computational theory of hippocampal function, and tests of the theory: new developments. Neurosci Biobehav Rev 48:92–147. CrossRef Medline

Klausnitzer J, Manahan-Vaughan D (2008) Frequency facilitation at mossy fiber–CA3 synapses of freely behaving rats is regulated by adenosine a1 receptors. J Neurosci 28:4836–4840. CrossRef Medline

Kowalski J, Gan J, Jonas P, Pernía-Andrade AJ (2016) Intrinsic membrane properties determine hippocampal differential firing pattern in vivo in anesthetized rats. Hippocampus 26:668–682. CrossRef Medline

Lanore F, Labrousse VF, Szabo Z, Normand E, Blanchet C, Mulle C (2012) Deficits in morphofunctional maturation of hippocampal mossy fiber synapses in a mouse model of intellectual disability. J Neurosci 32:17882–17893. CrossRef Medline

Lee AK, Epsztein J, Brecht M (2009) Head-anchored whole-cell recordings in freely moving rats. Nat Protoc 4:385–392. CrossRef Medline

Lorteije JA, Rusu SI, Kushmerick C, Borst JG (2009) Reliability and precision of the mouse calyx of held synapse. J Neurosci 29:13770–13784. CrossRef Medline

Marchal C, Mulle C (2004) Postnatal maturation of mossy fibre excitatory transmission in mouse CA3 pyramidal cells: a potential role for kainate receptors. J Physiol 561:27–37. CrossRef Medline

Margrie TW, Brecht M, Sakmann B (2002) In vivo, low-resistance, whole-cell recordings from neurons in the anaesthetized and awake mammalian brain. Pflugers Arch 444:491–498. CrossRef Medline

McBain CJ (2008) Differential mechanisms of transmission and plasticity at mossy fiber synapses. Amsterdam: Elsevier.

Mori M, Abegg MH, Gähwiler BH, Gerber U (2004) A frequency-dependent switch from inhibition to excitation in a hippocampal unitary circuit. Nature 431:453–456. CrossRef Medline

Mori M, Gähwiler BH, Gerber U (2007) Recruitment of an inhibitory hippocampal network after bursting in a single granule cell. Proc Natl Acad Sci U S A 104:7640–7645. CrossRef Medline

Nicoll RA, Schmitz D (2005) Synaptic plasticity at hippocampal mossy fibre synapses. Nat Rev Neurosci 6:863–876. CrossRef Medline

Paladini CA, Tepper JM (1999) GABA(A) and GABA(B) antagonists differentially affect the firing pattern of substantia nigra dopaminergic neurons in vivo. Synapse 32:165–176. CrossRef Medline

Pernía-Andrade AJ, Jonas P (2014) Theta-gamma-modulated synaptic currents in hippocampal granule cells in vivo define a mechanism for network oscillations. Neuron 81:140–152. CrossRef Medline

Price CJ, Scott R, Rusakov DA, Capogna M (2008) GABAB Receptor modulation of feedforward inhibition through hippocampal neurogliaform cells. J Neurosci 28:6974–6982. CrossRef Medline

Rollenhagen A, Sätzler K, Rodríguez EP, Jonas P, Frotscher M, Lübke JH (2007) Structural determinants of transmission at large hippocampal mossy fiber synapses. J Neurosci 27:10434–10444. CrossRef Medline

Rolls ET, Treves A (2011) The neuronal encoding of information in the brain. Prog Neurobiol 95:448–490. CrossRef Medline

Sachidhanandam S, Blanchet C, Jeantet Y, Cho YH, Mulle C (2009) Kainate receptors act as conditional amplifiers of spike transmission at hippocampal mossy fiber synapses. J Neurosci 29:5000–5008. CrossRef Medline

Salin PA, Scanziani M, Malenka RC, Nicoll RA (1996) Distinct short-term plasticity at two excitatory synapses in the hippocampus. Proc Natl Acad Sci U S A 93:13304–13309. CrossRef Medline

Schmidt-Hieber C, Jonas P, Bischofberger J (2004) Enhanced synaptic plasticity in newly generated granule cells of the adult hippocampus. Nature 429:184–187. CrossRef Medline

Szabadics J, Soltesz I (2009) Functional specificity of mossy fiber innervation of GABAergic cells in the hippocampus. J Neurosci 29:4239–4251. CrossRef Medline

Tamás G, Lorincz A, Simon A, Szabadics J (2003) Identified sources and targets of slow inhibition in the neocortex. Science 299:1902–1905. CrossRef Medline

Torborg CL, Nakashiba T, Tonegawa S, McBain CJ (2010) Control of CA3 output by feedforward inhibition despite developmental changes in the excitation-inhibition balance. J Neurosci 30:15628–15637. CrossRef Medline

Wilke SA, Antonios JK, Bushong EA, Badkoobehi A, Malek E, Hwang M, Terada M, Ellisman MH, Ghosh A (2013) Deconstructing complexity: serial block-face electron microscopic analysis of the hippocampal mossy fiber synapse. J Neurosci 33:507–522. CrossRef Medline